CHAPTER III
MATERIALS AND METHODS

In this chapter, a discussion of the different synthesis techniques, the main synthesis method for the experiments used in the present work, and a description of the experimental procedures used for the characterization studies are included.

3.1. Synthesis Techniques

Several techniques have been developed and are used for synthesizing nanomaterials. Broadly, these methods can be divided into vapour deposition techniques and solution-based chemistry techniques. Under vapour deposition, it is of two kinds viz physical vapour deposition and chemical vapour deposition and each method can be subdivided into more specific individual techniques. A process involving physical vapour deposition (PVD) describes the solidification of a vapour, in this case vapour created through thermally evaporating an II-VI compound source, directly onto a surface. This direct deposition implies that no chemical reactions are permitted to occur either in the vapour or with the vapour and the surface to be deposited on. If a chemical reaction does occur, then the process is not PVD, but rather a chemical vapour deposition (CVD) process. These synthesis techniques represent the majority of all techniques used for synthesizing nanomaterials, summarized in Table 3.1. (Gao *et al*., 2005)

Among them, the solvent growth technique is very effective in yielding a desirable size distribution and optimization of the physical properties. For investigation the materials are synthesized using chemical bath deposition technique.

Table 3.1: Several synthesis techniques of ZnO nanomaterials

Physical Vapour Deposition (PVD)	*Thermal Evaporation* i) Electron-beam ii) RF Induction iii) Resistive
	Sputtering i) Focused Ion Beam ii) Radio Frequency iii) Magnetron Sputtering
	Pulsed Laser Deposition
Chemical Vapour Deposition (CVD)	i) Thermal CVD ii) Low-pressure CVD (LPCVD) iii) Plasma-enhanced CVD (PECVD) iv) Metal-organic CVD (MOCVD) v) Molecular Beam Epitaxy (MBE) vi) Atomic Layer Deposition (ALD)
Solution Chemistry (SC)	i) Colloidal Chemical Method ii) Electro Deposition Method iii) Sol-Gel iv) Reversed Micelles v) Copolymer Micelles vi) Chemical bath deposition

3.2. Physical Vapour Deposition Methods

In physical vapour deposition process, vapour is created and it is deposited on a deposition substrate by a physical process. The three most important techniques for ZnO deposition are thermal evaporation, sputtering, and pulsed laser deposition. Each of these will be described below, but they share in common that the source material is the same as the intended depositing material and no chemical reactions occur throughout the process.

3.2.1. Thermal Evaporation Technique

Thermal evaporation is one of the most common and simple techniques of forming II-VI nanomaterials. During a basic thermal evaporation process, the substrate and source materials are placed inside a vacuum chamber. This vacuum can reach pressures as low as 10^{-9} torr (an ultra-high vacuum). A heating source is used to heat the source material to its vapour point or above. The condensed or powder source material is vapourized at elevated temperatures and then the resultant vapour phase(s) condenses under certain conditions (temperature, pressure, atmosphere, etc) to form a desired product along the substrate in the cooler area of the vacuum chamber. The main difference in the types of thermal evaporation techniques is with the type of heating used to vapourize the source material. Some examples of heating sources are electron-beam, radio frequency (RF) induction, and resistive heating.

Electron beam evaporation is based on the heat produced by high energy electron beam bombardment on the material to be deposited. The electron beam is generated by an electron gun, which uses the thermionic emission of electrons produced by an incandescent filament (cathode). Emitted electrons are accelerated towards an anode by a high difference of potential. The crucible itself or a near perforated disc can act as the anode. A magnetic field is often applied to bend the electron trajectory, allowing the electron gun to be positioned below the evaporation line. As electrons can be focalized, it is possible to obtain a much localized heating on the material to evaporate, with a high density of evaporation power. In comparison, RF induction uses an alternating current through an induction coil to heat the source material. This current produces a magnetic field which induces eddy currents in the source material. This provides localized heating without any physical contact between the coil and the source material. Resistive heating provides heat by sending an electrical current through a resistive coil and is a non-localized heat source as it heats the area around it as well. Therefore, it is commonly used for furnace applications. Resistive sources of heating are the most commonly used for thermal evaporation and have created a variety of ZnO nanostructures (Liua *et al*., 2005, Yao *et al*., 2002, Senthil Kumar *et al*., 2011, Srivastava *et al*., 2011, Chrissanthopoulos *et al*., 2007).

3.2.2. Sputtering

Sputtering is a physical process whereby atoms in a solid target material are ejected into the gas phase due to bombardment of the material by energetic ions. The ions for the sputtering process are supplied by induced plasma. A variety of specific sputtering techniques are used to modify the properties of this plasma, and thus achieve different sputtering conditions, including direct current (DC), radio-frequency (RF), magnetron (which utilizes magnetic fields), focused ion-beam, and application of a bias voltage to the target. A schematic of sputter deposition is shown in Figure 3.1.

In general, the simplest form of sputtering is DC sputtering, where the substrate and target material are placed inside a vacuum chamber. An inert gas such as argon is introduced and a DC power supply is used to ionize the gas. The ions are then accelerated towards the target, breaking off the surface atoms of the target. These atoms then condense on a deposition substrate. When applied to ZnO, sputtering produce polycrystalline thin films successfully. (Arroyo-Hernández *et al*., 2011, Amir Abdallah *et al*., 2011, Flickyngerová *et al*., 2006).

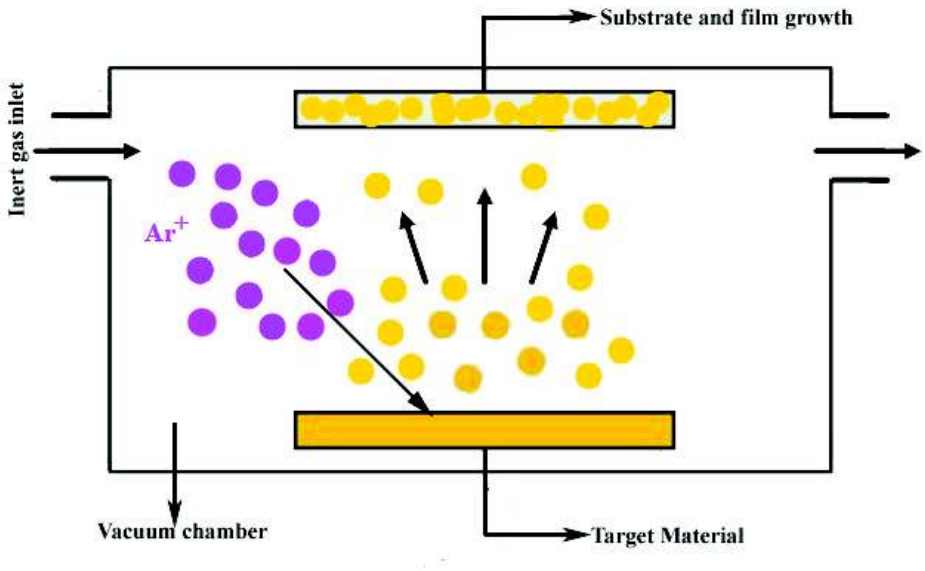

Figure 3.1: A schematic of sputtering deposition process

An advantage of sputtering as a deposition technique is that the deposited films have the same composition as the source material. The equality of the film and target stoichiometry might be surprising since the sputter yield depends on the atomic weight

of the atoms in the target. One might therefore expect one component of an alloy or mixture to sputter faster than the other components, leading to an enrichment of that component in the deposit. However, since only surface atoms can be sputtered, the faster ejection of one element leaves the surface enriched with the others, effectively counteracting the difference in sputter rates. In contrast with thermal evaporation techniques one component of the source may have a higher vapour pressure, resulting in a deposited film with a different composition than the source.

3.2.3. Pulsed Laser Deposition

During pulsed laser deposition (PLD), a high power laser beam is focused inside a vacuum chamber and forced to strike a target of the desired composition. This vaporizes the material from the target, producing a plume of material with a stoichiometry similar to that of the target material. The vapour plume then deposits onto a cooler deposition substrate that promotes the nucleation and growth of the desired material. Though PLD is typically used to produce crystalline films, it has been used successfully to produce one-dimensional nanostructures as well. With ZnO, PLD has been used to form thin film (Christian *et al*., 2011, Sang Hyuck Bae *et al*., 2000). A schematic of the PLD process is shown in Figure 3.2. PLD can be performed in several different types of chambers. All that is required is a vacuum chamber, a place for the target material, the deposition substrates, and a window through which the laser beam can be transmitted.

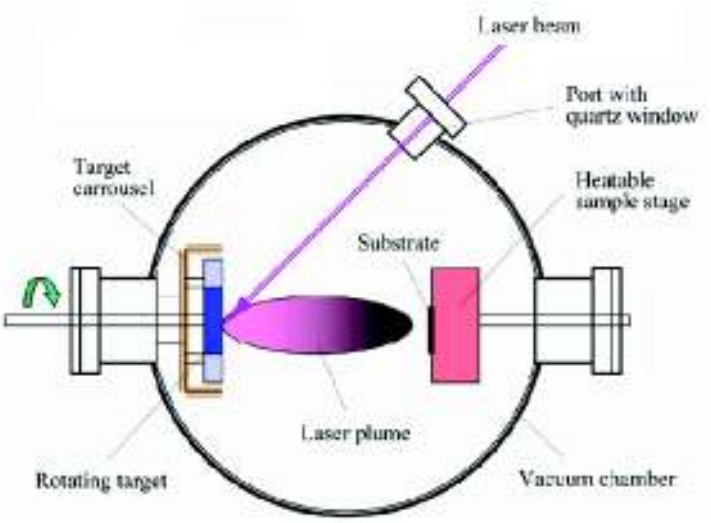

Figure 3.2: A schematic of a typical Pulsed Laser Deposition process

3.3. Chemical Vapour Deposition Methods

In chemical vapour deposition (CVD) process one or more volatile precursors chemically react and/or decompose on the substrate surface to produce the desired nanomaterials. CVD processes differ from PVD in that a chemical reaction is necessary in creating the desired stoichiometry in CVD whereas in PVD the desired stoichiometry is similar to the source material. Frequently, volatile byproducts of the chemical reaction are produced. Among the more common CVD techniques used to deposit ZnO is thermal CVD, molecular beam epitaxy (MBE), and atomic layer deposition (ALD). In each of these techniques, a vacuum chamber with a gas flow is required.

3.3.1. Thermal Chemical Vapour Deposition

Thermal CVD requires pressure near 10^{-3} torr and reactions occur sometimes in excess of 900°C between the supplied gases. Thermal CVD can occur between two gas phase precursors or between a gas phase precursor and a solid phase precursor. Thermal CVD is typically used to form thin films and it is limited by its high required temperatures and the slow deposition rates. However, the method has recently been shown to be able to synthesize ZnO nanotube arrays, ZnO nanoribbons and tetrahedral nano ZnO (An-Jen Cheng *et al*., Feng Shi *et al*., 2012, Wan *et al*., 2010).

3.3.2. Molecular Beam Epitaxy

In solid-source Molecular Beam Epitaxy (MBE), ultra-pure elements such as gallium and arsenic are heated in separate quasi-knudsen effusion cells until they each slowly begin to evaporate. The evaporated elements then condense on the wafer, where they may react with each other. This forms single-crystal gallium arsenide. The process takes place in high vacuum or ultra high vacuum. The term "beam" simply means that evaporated atoms do not interact with each other or any other vacuum chamber gases until they reach the wafer, due to the large mean free path lengths of the beams. A schematic of MBE is shown in Figure 3.3.

The most important aspect of MBE is the slow deposition rate, which allows the films to grow epitaxially. However, the slow deposition rates require proportionally better vacuum in order to achieve the same impurity levels as other deposition techniques. A computer controls shutters in front of each furnace, allowing precise

control of the thickness of each layer, down to a single layer of atoms. Intricate structures of layers of different materials may be fabricated this way. MBE has been able to form a variety of ZnO nanostructures, including tetrapod nanocrystals, quantum dots and ZnO films (Belmoubarik *et al*., 2013, Kwang Gug Yim *et al*., 2011, Tang *et al.,* 1998, Ko *et al*., 2000).

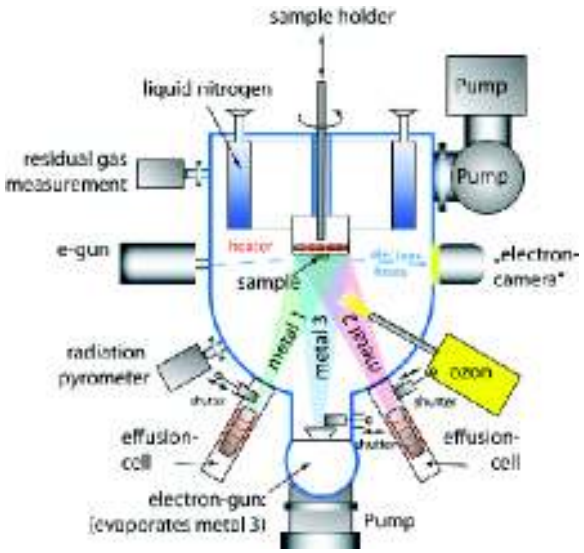

Figure 3.3: A schematic representation of MBE chamber

3.3.3. Atomic Layer Deposition

Atomic Layer Deposition (ALD) is a Chemical Vapour Deposition (CVD) process in which two complementary materials are alternatively introduced into the reaction chamber. The premise behind the ALD process is a simple one. The substrate (amorphous or crystalline) is exposed to the first gaseous precursor molecule (elemental vapour or volatile compound of the element) in excess and the temperature and gas flow is adjusted so that only one monolayer of the reactant is chemisorbed onto the surface (Figure 3.4(a)). The excess of the reactant, which is in the gas phase or physisorbed on the surface, is then purged out of the chamber with an inert gas pulse before exposing the substrate to the other reactant (Figure 3.4(b)). The second reactant then chemisorbs and undergoes an exchange reaction with the first reactant on the substrate surface (Figure 3.4(c)). These results in the formation of a solid molecular film and a gaseous side product that may then be removed with an inert gas pulse (Figure 3.4(d)). Thus the film thickness is controlled by the number of precursor

cycles rather than the deposition time as is the case for conventional CVD processes. In theory ALD allows for atomic level control of thin film thickness and uniformity.

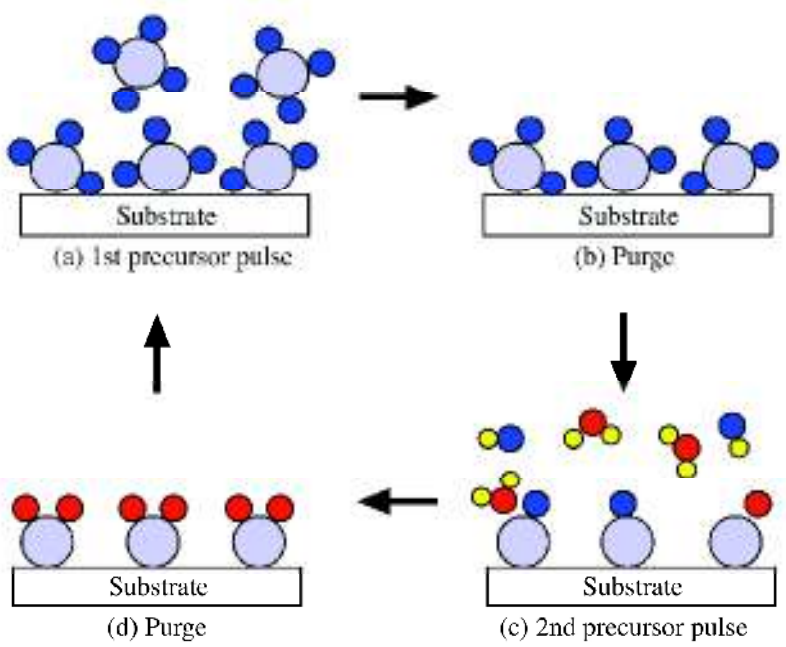

Figure 3.4: A schematic representation of an ALD process

ZnO films were deposited on Si (100) substrates by ALD. Diethylzinc (DEZn) was used as the precursor for zinc and deionized water was used as the oxidation source. The growth cycle consists of precursor exposures and N_2 purge following the sequence of DEZn/N_2/H_2O/N_2. DEZn and H_2O were fed into the chamber through separate inlet lines and nozzles. In the ALD method, reagents (precursors) are introduced sequentially into the growth chamber and when precursors reach the substrate, they are interspersed by cycles of purging with inert gas (N_2). The pressures of the DEZn and H_2O in the reactor chamber were approximately 1 and 2 Torr, respectively, monitored by a vacuum gauge. The substrate temperature was maintained at 177 °C during the deposition (Yumi Kawamura *et al*., 2011; Francisco Solís-Pomar *et al*., 2011).

3.4. Solution Based Chemistry

Any chemical reaction that requires a solution to occur is a form of solution based chemistry (SBC). Often, some materials with complex stoichiometries are difficult to synthesize via vapour deposition techniques. In these situations, SBC has served as

a vital technique in producing these materials. SBC techniques typically provide materials with high yield and uniformity, but a major disadvantage is that there are more point, line, and planar defects than there are in vapour deposition created materials.

However, there are certain difficulties in chemical processing. In some preparations, the chemistry is complex and hazardous. Contamination can also result from the byproducts being generated or side reactions in the chemical process. This should be minimized or avoided to obtain desirable properties in the final product. Agglomeration can also be a major cause of concern at any stage in a synthetic process and it can dramatically alter the properties of the materials. As an example, agglomeration frequently makes it more difficult to consolidate nanoparticles to a fully dense compact. Finally, many chemical processes are scalable for economical production but it is not always straight forward for all systems.

Solution based chemistry is used sometimes to prepare the precursor, which is subsequently converted to the nanophase particles by non-liquid phase chemical reaction. Precipitation of a solid from a solution is a common technique for the synthesis of fine particles. The general procedure involves reactions in aqueous or non-aqueous solutions containing the soluble and suspended salts. Once the solution becomes supersaturated with the product, the precipitate is formed by either homogeneous or heterogeneous nucleation. The formation of a stable material with or without the presence of a foreign species is referred to as heterogeneous or homogeneous nucleation (Overbeek 1982). The growth of the nuclei after formation usually proceeds by diffusion, in which case concentration gradients and reaction temperatures are very important in determining the growth rate of the particles, for example, to form monodispersed particles. For instance, to prepare unagglomerated particles with a very narrow size distribution all the nuclei must form at nearly the same time and subsequent growth must occur without further nucleation or agglomeration of the particles.

The most important techniques for ZnO synthesis are the colloidal chemical method, electro deposition method, sol-gel process, reversed micelles, copolymer micelles and microwave irradiation technique.

3.4.1. Colloidal Chemical Method

The most common approach to the synthesis of colloidal quantum dots (QDs) is the controlled nucleation and growth of particles in a solution of chemical precursors containing the metal and the anion sources (controlled arrested precipitation). The technique of forming monodisperse colloids is very old. A common method for II-VI colloidal QD formation is to rapidly inject a solution of chemical reagents containing the group II and VI species into hot and vigorously stirred solvent containing molecules that can coordinate with the surface of the precipitated QD particles (Nalwa (Ed.) 2002). Consequently, a large number of nucleation centers are initially formed, and the coordinating ligands in the hot solvent prevent or limit particle growth via Ostwald ripening (the growth of larger particles at the expense of smaller particles to minimize the higher surface free energy associated with smaller particles).

Further improvement of the resulting size distribution of the QD particle can be achieved through selective precipitation, whereby the slow addition of a capping agent (stabilizer) to the colloidal solutions of growing clusters prevents further growth of these materials by covalently binding to the cluster surface. Thiolates are the most commonly used capping agents and this method also forms the basis of the synthesis of monodispersed clusters of CdS. The schematic diagram for the synthesis of thiophenolate capped CdS clusters is shown in Figure 3.5. To use the colloidal chemical method for the synthesis of QDs, it is important that the stabilizer and solvent do not decompose during reaction time in order to ensure good solubility of QDs after synthesis and to avoid formation of different trapping states on the surface.

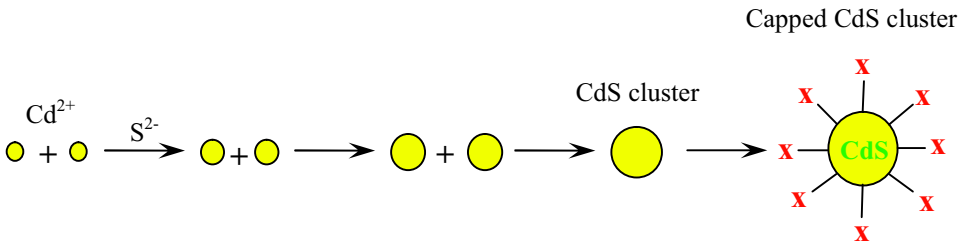

Figure 3.5: Schematic diagram for the synthesis of thiophenolate capped CdS clusters (X represents the thiophenolate ion; the size of the circle represents the size of the CdS clusters. The growth of the CdS clusters is analogous to the growth of a polymer as long as the surfaces are not covered by the terminating agent X)

One of the first attempts to produce II-VI nanocrystals was the manufacture of colloidal suspensions where, for example, CdS was formed by precipitation of Cd^{2+} in aqueous solution by adding H_2S. Additionally, a small amount of sodium polyphosphate was added for stabilization. When carrying out the reaction with an excessive Cd^{2+} concentration, a surface passivation was observed by formation of a $Cd(OH)_2$ layer (Rodríguez-Paéz *et al*., 2001, Yizheng Jin *et al*., 2008). CdS crystallites could be grown down to very small sizes. The existence of very small stable CdS super clusters (55 atoms) could be demonstrated with astonishingly regular shape and small pyramids (Horst Weller 2003, Changle Wu *et al*., 2006).

3.4.2. Electrodeposition

Nanostructure materials can also be produced by electrodeposition. These films are mechanically strong and uniform. Substantial progress has been made in nanostructure coatings applied either by DVD or CVD. Many other non-conventional processes such as hypersonic plasma particle deposition (HPPD) have been used to synthesize and deposit nanoparticles. The significant potential of nanomaterial synthesis and their applications is virtually unexplored. They offer numerous challenges to overcome. Understanding more of synthesis would help in designing better materials. It has been shown that certain properties of nanostructure deposits such as hardness, wear resistance and electrical resistivity are strongly affected by grain size. A combination of increased hardness and wear resistance results in a superior coating performance. Electrodeposition method has been able to form a variety of ZnO and doped ZnO nanostructures, including nanotubes and nanowires (Xingtian Yin *et al*., 2011, Shuxi Dai *et al*., 2013).

3.4.3. Sol-Gel Techniques

Sol-Gel techniques incorporate the creation of inorganic networks through the formation of a colloidal suspension in a liquid (sol) and gelation of the solution to form a network in a continuous liquid phase (gel). Precursors for creating these colloids are metal/metalloid surrounded by various reactive ligands. A catalyst is used to start reaction and control pH. Sol-gel formation occurs in four stages.

- Hydrolysis
- Condensation

- Growth of particles
- Agglomeration of particles

The sol-gel process allows the fabrication of materials with a large variety of properties: ultra-fine powders, monolithic ceramics and glasses, ceramic fibers, inorganic membranes, thin film coatings and aerogels. The sol-gel process has been used to create nanoscale particles of ZnO for phosphor applications (Chander 2005).

In general, the particle size and particle size distribution, the physical properties such as crystallinity and crystal structure and the degree of dispersion can be affected by reaction kinetics. In addition the concentration of reactions, the reaction temperature, the pH and the order of addition of reactants to the solution are also important. Even though a multi element material is often made by co-precipitation of batched ions; it is not always easy to co-precipitate at different pH. Thus, control of chemical homogeneity and stoichiometry requires a very careful control of reaction conditions. The problem of agglomeration may be avoided in liquid phase reactions by common methods such as spray drying and freeze drying (Nielsen 1982, Real 1986).

Semiconductor clusters have traditionally been prepared by the use of micelles/reversed micelles, copolymer micelles, crystalline hosts and glasses (Nalwa (Ed.) 2002). The clusters prepared by these methods have poorly defined surfaces and a broad size distribution, which is detrimental to the properties of the semiconductor material. The synthesis of monodisperse clusters with very well defined surfaces is still a challenge to synthetic chemists. However, some of the recent approaches used to overcome these problems are: i) the synthesis of clusters within a porous host lattice (such as zeolite) acting as a template and ii) the controlled fusion of clusters.

3.4.4. Chemical Bath Deposition

Chemical bath deposition (CBD) (Mitra *et al*., 1998, Dong *et al*., 1997, Chang *et al*., 2002, Ito *et al*., 1995) is one of the solution phase methods useful for the preparation of compound semiconductors from aqueous solutions. A chemical bath deposition method (CBD) is also called as solution growth, controlled or arrested precipitation, electroless deposition etc. It is widely used for the deposition of various metal chalcogenide and oxide thin films. It produces good deposits on suitable substrates by the controlled precipitation of the compounds from the solution. The

method offers many advantages over other well-known vapour phase synthetic routes. It may allow us to easily control the growth factors such as film thickness, deposition rate and quality of crystallites by varying the solution pH, temperature and bath concentration (Sberveglieri 1995). It does not require high voltage equipment, works at room temperature, and hence it is inexpensive. The only requirement for this deposition route is an aqueous solution consisting of a few common chemicals and a substrate for the film to be deposited. It often suffers from a lack of reproducibility in comparison with other chemical processes; however, by the proper and careful optimization of the growth parameters, reasonable reproducibility can be obtained.

The major problem of the CBD method is the inefficiency of the process which converts the precursor materials into useful deposits. Two types of nucleation take place in solution: homogeneous nucleation and heterogeneous nucleation. Homogeneous nucleation leads to rapid formation of large particles throughout the solution, as precipitate. Conversely, heterogeneous nucleation occurs at the substrate surface and particles grow slowly to form a film. The heterogeneous growth of the film on the substrate is disrupted by the competing homogeneous reaction in solution and the subsequent deposition on the surface of the vessel containing the solution bath. This difficulty is avoided by using a pre-treated substrate for the formation of seed layers or by employing the successive ionic layer adsorption and reaction (SILAR) method. Growing of a ZnO thin film on a glass substrate from an alkaline solution requires a seed layer. However, the deposition of ZnO thin film on a zinc plate does not require a seed layer, unlike other substrates such as glass, ITO or Fluorine doped tin oxide (FTO).

The advantages of chemical bath deposition method are discussed below (Suryanarayana *et al*., 1986, Sharma *et al*., 1979):

i. The method does not require sophisticated instrumentation.
ii. It is applicable for large area deposition.
iii. Electrical conductivity of the substrate materials is not an important criterion.
iv. The deposition is easy even at low temperature and avoids the oxidation or corrosion of the metallic substrate.
v. An intimate contact between reacting solution and substrate gives pinhole free and uniform deposition.
vi. Stoichiometry of the deposit can be easily maintained.

vii. The process is slow that facilitates better orientation of crystallites with improved grain structure.

viii. The method can be used to deposit a large number of metal chalcogenides.

ix. As very dilute solutions are used in the process, the method offers minimum toxicity and occupational hazards.

3.5. Preparation of ZnO Film

The technique that is used for the experiments in the present work is a simple chemical bath deposition technique. A schematic diagram of chemical bath deposition method is shown in Figure. 3.6.

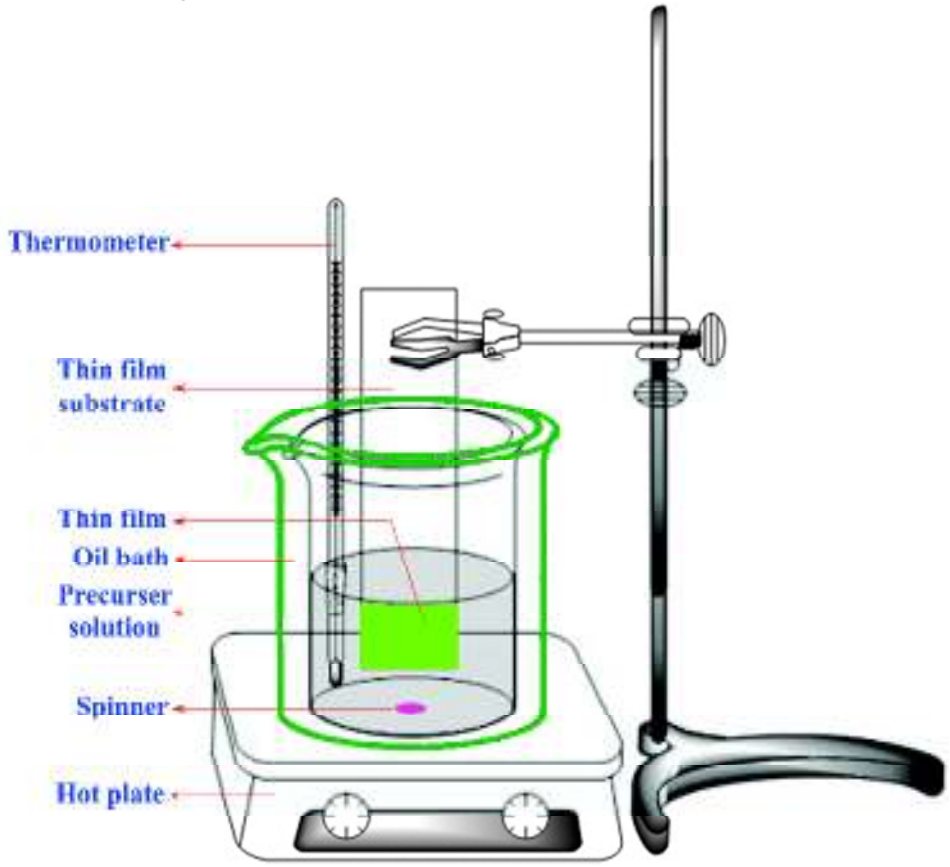

Figure 3.6: A schematic representation of chemical bath deposition system

3.5.1. A Dust Proof Chamber

A dust proof chamber was designed and fabricated using plywood with its dimension 2 x 1 x 0.5 m. In order to provide the clean and contaminant free environment for the deposition of samples, hollow pipe outlet at the top of the chamber

was fitted with an exhaust fan. This assembly also helps to remove the gases evolved during the thin film deposition.

3.5.2. Oil/water Bath

Paraffin oil/water in a metallic container was used as a bath. A thermometer was used to measure the temperature of the oil/water bath.

3.5.3. Reaction Vessel

A 'Scott Duran' made glass beaker of capacity 250/100 ml was used as the reaction vessel. The beaker was fitted in the oil bath by means of suitable ring stand. Each solution poured in the beaker was heated to 50 ºC and then mixed to form reactive mixture. The reaction mixture was maintained in the range of 60 ºC ± 1 ºC temperature in the oil/water bath.

3.5.4. Substrate Cleaning

Substrate cleaning is the process of breaking the bonds between substrates and contaminants without damaging the substrates. In thin film deposition process substrate cleaning is an important factor to get reproducible films as it affects the smoothness, uniformity, adherence and porosity of the films. The substrate cleaning process depends upon the nature of the substrate; degree of cleanliness required and nature of contaminates to be removed. The common contaminates are grease, adsorbed water, air borne dust, lint, oil particles etc. The micro slides supplied by Blue Star of dimensions 7.5 cm x 2.2 cm x 0.1 cm have been used as the substrates.

The following process has been adopted for cleaning the substrates.

i. The substrates were washed with detergent solution 'Labolene' and then with water.
ii. These substrates were boiled in chromic acid for about ten minutes.
iii. Substrates were cleaned with double distilled water.
iv. These substrates were kept in NaOH solution to remove the acidic contaminations.
v. The substrates were again washed with distilled water and cleaned ultrasonically.

vi. Finally substrates were dried in alcohol vapours.

3.5.5. Preparation Technique

Zinc acetate and urea were used as the starting materials. Ammonium solution was used to maintain the pH at 9. Pure ZnO thin film was prepared from the precursor materials taken in 1:1 molar ratio and dissolved in 50ml double distilled water. Heating the liquid phase at 60 ºC with continuous stirring yield the ZnO particle in average nano meter size. Now the cleaned glass substrate is immersed in the above processed solution to coat over the substrate. This method is based on the sequence of reaction on the substrate surface. ZnO is formed by the following reaction

$$(CH_3COO)_2Zn \rightarrow 2CH_3COO^- + Zn^{2+}$$

$$NH_2CONH_2 + H_2O \longrightarrow 2NH_3 + CO_2$$

$$2NH_3 + CO_2 + 2H_2O \longrightarrow 2NH_4^+ + 2OH^-$$

$$Zn^{2+} + 2NH_4^+ + 2OH^- \longrightarrow Zn(OH)_2$$

$$Zn(OH)_2 \longrightarrow ZnO + H_2O$$

The coating time is varied from 30 min to 3 h in order to vary the thickness of the ZnO films. The impurities added in ZnO films are Manganese chloride, Copper chloride and Lead chloride with the above sol in different concentrations namely 2.5, 5.0, 7.5 and 10 mole%. Figure 3.7 contain the photographs of synthesized pure and doped ZnO thin films.

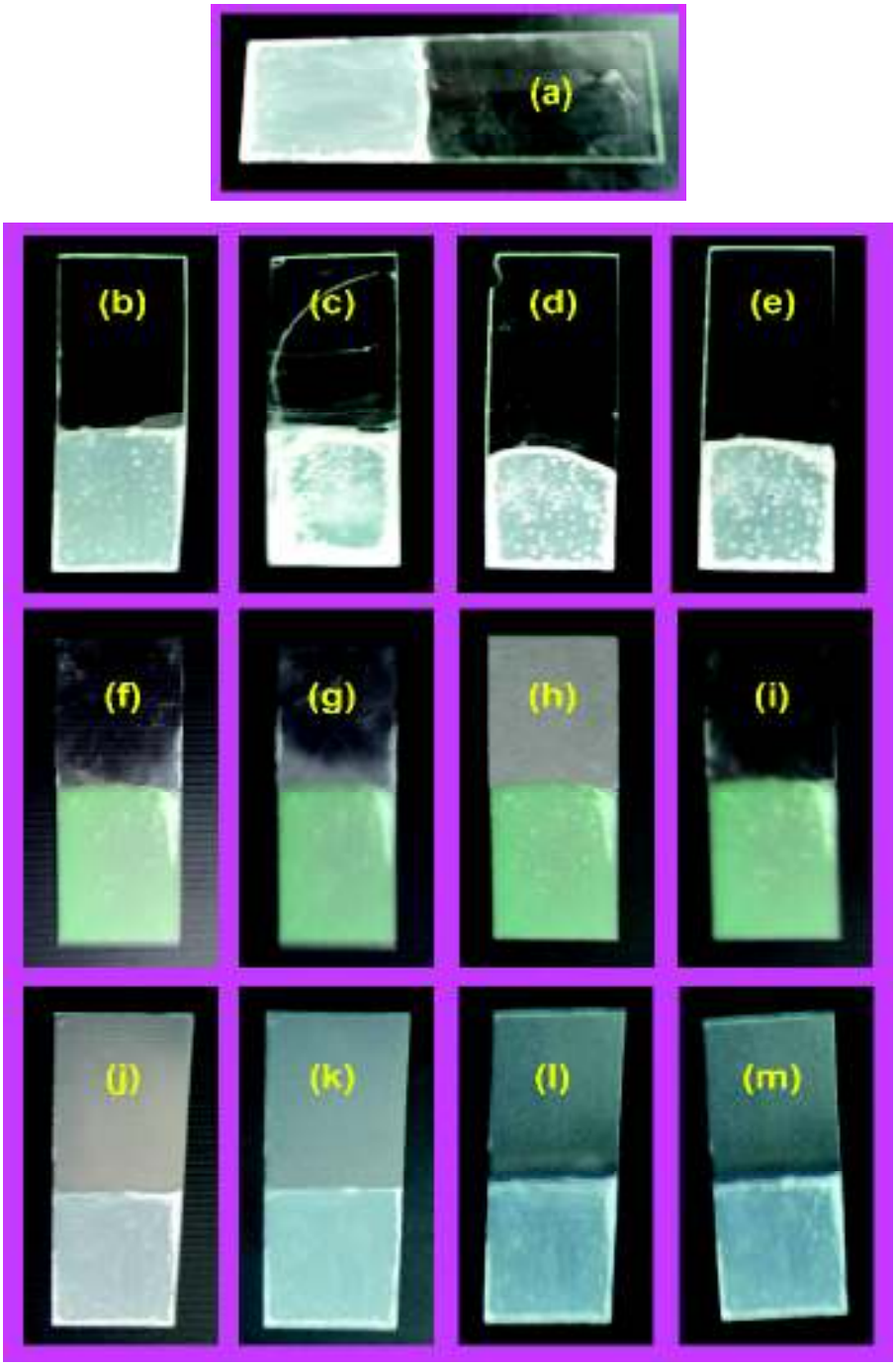

Figure 3.7: Photograph of the synthesized (a) pure ZnO (b) 2.5 mole % Mn^{2+} doped ZnO (c) 5.0 mole % Mn^{2+} doped ZnO (d) 7.5 mole % Mn^{2+} doped ZnO (e) 10.0 mole % Mn^{2+} doped ZnO (f) 2.5 mole % Cu^{2+} doped ZnO (g) 5.0 mole % Cu^{2+} doped ZnO (h) 7.5 mole % Cu^{2+} doped ZnO (i) 10.0 mole % Cu^{2+} doped ZnO (j) 2.5 mole % Pb^{2+}

doped ZnO (k) 5.0 mole % Pb^{2+} doped ZnO (l) 7.5 mole % Pb^{2+} doped ZnO (m) 10.0 mole % Pb^{2+} doped ZnO nanocrystalline films

3.6. Characterization of Pure, Mn^{2+}, Cu^{2+} and Pb^{2+} Doped ZnO Nanocrystals

Characterization includes powder X-ray diffraction (PXRD) measurements, Atomic force microscopy (AFM) measurements, Scanning electron microscopy (SEM) measurements, Transmission electron microscopy (TEM) measurements, Energy dispersive X-ray absorption (EDAX) analysis, optical measurements, Photoconductivity measurements and electrical measurements.

3.6.1. XRD Measurement

X-ray diffraction (XRD) is an important technique in the characterization of materials to obtain structural information on an atomic scale from both crystalline and non-crystalline (amorphous) materials. X-ray powder diffraction is an instrumental technique that is normally used to study crystalline materials. The three dimensional structure of non – amorphous materials is defined by regular, repeating planes of atoms that form a crystal lattice. When a focused x-ray beam interacts with these planes of atoms, part of the beam is transmitted, part is absorbed by the sample, part is refracted and scattered, and part is diffracted.

When an X-ray beam hits a sample and is diffracted, we can measure the distance between the planes of the atoms that constitute the sample by applying Bragg's law, $n\lambda = 2d \sin\theta$, where the integer n is the order of the diffracted beam, λ is the wavelength of the incident X-ray beam, d is the distance between adjacent planes of the atoms (the d-spacing), and θ is the angle of incidence of the X-ray beam. Subsituting the value of λ we can measure θ, and calculate d-spacing. The characteristic set of d-spacing and their intensity generated in a typical X-ray scan provide ample information. When properly interpreted, by comparison with standard reference patterns and measurements, this "finger print ˝ allows for identification of the material. Presence of an amorphous material in the sample can be determined by occurrence of wide halo on diffraction pattern.

The ease and precision with which X-ray intensity measurements are made by means of fully automated diffractometer has greatly contributed to the growth of successful crystal structure analysis. From the X-ray powder diffraction data we can get

the angle of scattering and the corresponding intensities of diffracted beams for each reflection. Lattice parameters can be obtained from this data. Also, the data can be used to check for any lattice distortion. The schematic diagram of XRD is shown in Figure 3.8.

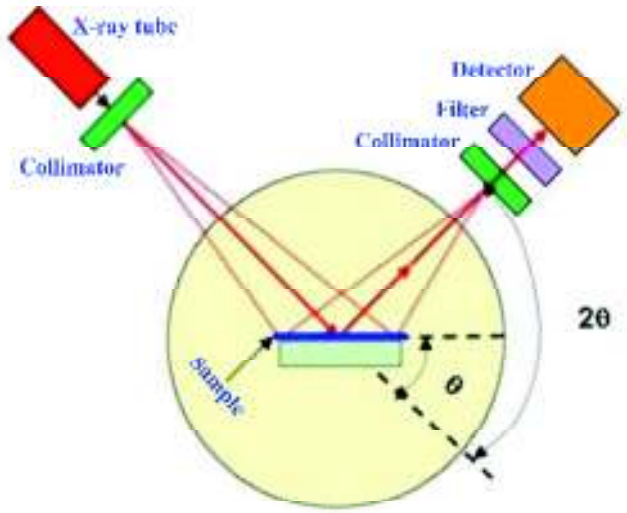

Figure 3.8: Schematic diagram of XRD system

In order to confirm the material of the grown crystals and to determine the particle size, powder X-ray diffraction (PXRD) data were collected for all the fourteen nanocrystals prepared using an automated x-ray powder diffractometer (PANalytical) in the 2θ range of 10-70° with CuK_{α} radiation (λ = 1.54056 Å). Using the observed 2θ (Bragg angle) and d (interplanar spacing), all the reflections were indexed. Indexing a PXRD pattern consists of the assignment of three numbers h k l (Miller indices) to each reflection. The data were indexed following the procedures of Lipson and Steeple (1970). ZnO nanocrystals belong to the cubic lattice system. The observed PXRD data for ZnO and ZnO doped with Mn^{2+}, Cu^{2+} and Pb^{2+}nanocrystal thin films were indexed by matching with the data available in the literature and JCPDS file (Xichang Bao *et al*., 2013, Sarvari Khatoon *et al*., 2013, Durgajanani Sivalingam *et al*., 2012, PCPDFWIN database version 2.4, JCPDS File no. 36-1451 (2003). Since an X-ray diffraction pattern is determined by the atomic arrangement within a specimen, any material will produce a diffraction pattern that is characteristic of its constituent compounds or phases. Identification is aided by search and match software which compares experimental data with standard patterns from the ICDD reference database (JCPDS

file). From this comparison we can identify the compounds and phases of the synthesized materials.

The broadening of X-ray diffraction peaks provides a convenient method for measuring particle sizes below 0.1 micrometer. The origins of the X-ray line broadening effects, like many other diffraction effects of crystals is best understood in terms of reciprocal lattices. Essentially, the width of the diffraction peak is inversely proportional to parameter that is a measure of the size of the crystallites. When the size of the crystallites increases, the width of the peak decreases. If the crystallite gets too large, greater than 0.1 micron in average diameter the peaks are so narrow that the width cannot be distinguished from the broadening in the X-ray diffraction instrument. In addition to size other factors such as lattice strain can produce broadening of X-ray peaks. However, for particle sizes below approximately 20 nm the broadening by size dominates. The sizes of the crystallites (d_{hkl}) were obtained from the Debye-Scherrer's equation (Cullity 1977).

Grain or crystallite sizes of the synthesizes nanoparticles were determined by the following Debye-Scherrer's equation

$$D = \frac{K\ \lambda}{\beta \cos\theta},$$

where D is the mean diameter (size) of the grains, K (= 0.9) is the size factor, β is the full width at half maximum (in radians), λ is the wavelength of the X ray radiation used and 2θ is the angle at which the maximum intensity was observed. Two to three diffraction peaks were chosen wherever possible and consistency in the cluster sizes obtained from using their widths was confirmed.

In our present study, crystallite sizes were calculated for all the synthesized samples using both Scherrer method and Voigt function method (Langford 1998). Scherrer method takes account of the width of the peak. But, since the area under the peaks consist information regarding the number of crystallites, the Voigt function method where the calculation relies on integral breadth (area/height) is of significant value for accurate crystallite size measurements (Yadav *et al* 2005; Chiche *et al*. 2008).

The effective crystallite sizes of the synthesized samples were calculated based on line broadening of XRD peaks. The use of the Voigt function for the analysis of the integral breadths of broadened X-ray diffraction line profiles forms the basis of a rapid

and powerful single line method of crystallite size determination. In this case, the constituent Couchy component can be obtained from the ratio of full width at half maximum intensity (2ω) and integral breadth (β) (Langford 1978)

$$D = \frac{\lambda}{\beta_C \cos\theta}$$

The constituent Couchy component can be given as

$$\beta_C = (a_0 + a_1 \psi + a_2 \psi^2)\ \beta$$

$$\psi = \frac{2\omega}{\beta}$$

Where a_0, a_1 and a_2 are Couchy constants and β is the integral breadth obtained from XRD peak.

$$\beta = \frac{\text{Area under the peak}}{\text{Height of the peak}}$$

The values of Couchy constants have been taken from the table of Langford (1978) a_0 = 2.0207, a_1 = −0.4803, a_2 = −1.7756. From these, we have calculated the crystallite size D.

The lattice constants 'a=b' and 'c' for wurtzite phase of pure ZnO and ZnO doped with 2.5, 5.0, 7.5 and 10 mole % of Zn^{2+}, Cu^{2+}, Pb^{2+} and Mn^{2+} nanocrystals were calculated using the following equation (Leonid *et al*., 1968),

$$\frac{1}{d^2_{(h\,k\,l)}} = \frac{4}{3}\left(\frac{h^2 + hk + k^2}{a^2}\right) + \frac{l^2}{c^2}$$

Where $d_{(h\,k\,l)}$ is the interplanner distance of the particular (h k *l*) plane which is observed from the powder XRD pattern.

3.6.2. Energy Dispersive X-ray Spectroscopy

In order to characterize the samples prepared chemically, it is necessary to determine accurately the metal atom (Zn, Mn, Cu and Pb) contents. As these samples are not soluble in water, atomic absorption spectroscopic (AAS) technique cannot be used for this. However, other techniques like energy dispersive X-ray absorption (EDAX) analysis can very well be utilized. It is an analytical technique used to estimate the composition of the prepared materials. It relies on the investigation of a sample through interactions between electromagnetic radiation and matter, analyzing x-rays

emitted by the matter in response to being hit with charged particles. Its characterization capabilities are due in large part to the fundamental principle that each element has a unique atomic structure allowing x-rays that are characteristic of an element's atomic structure to be identified uniquely from each other.

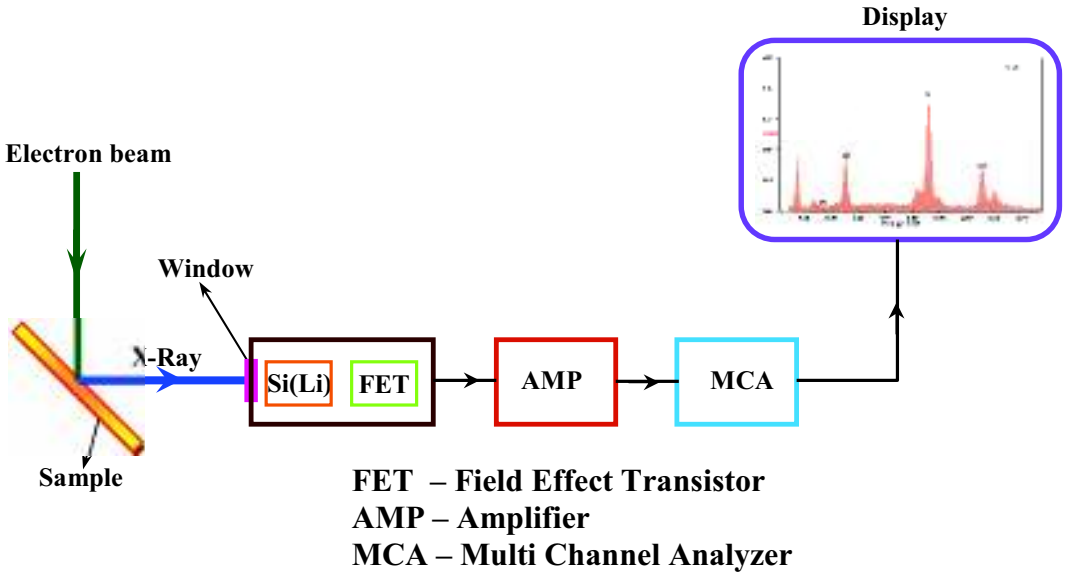

Figure 3.9: Schematic diagram of an EDAX system

Figure 3.9 shows a schematic diagram of an EDAX system. To stimulate the emission of characteristic X-rays from a specimen, a high energy beam of charged particles such as electrons or protons, or a beam of X-rays, is focused into the sample being studied. At rest, an atom within the sample contains ground state (or unexcited) electrons in discrete energy levels or electron shells bound to the nucleus. The incident beam may excite an electron in an inner shell, ejecting it from the shell while creating an electron hole where the electron was. An electron from an outer, higher-energy shell then fills the hole, and the difference in energy between the higher-energy shell and the lower energy shell may be released in the form of an X-ray. These X-rays pass through the window protecting the Si (Li) and are absorbed by the detector crystal. The X-ray energy is transferred by a field effect transistor (FET), and amplified (AMP) to a level that can be processed into a digital signal by the analog-to-digital converter (ADC) of the multichannel analyzer (MCA). By an energy calibration of the channels in the MCA, the collection of X-ray pulses is displayed as an energy histogram. EDAX systems are controlled by computers and are used for the basic operations of spectrum collection and peak identification. The X-ray spectra give information on the types of elements

present in a specimen from the wavelength of the X-ray emitted and the elemental concentration from the intensity of the particular peak.

The EDAX analysis was carried out for all the samples prepared in the present study using a Jeol make JSM 5600 LV Model attached with Energy Dispersive Spectrometer of EDAX inc. USA.

3.6.3. AFM Measurements

The AFM consists of a micro scale cantilever with a sharp tip (probe) at its end that is used to scan the specimen surface. The cantilever is typically silicon or silicon nitride with a tip radius of curvature on the order of nanometers. The probe is extremely close to but does not touch the surface. As the probe traverses the surface, attractive and repulsive forces arising between it and the atoms on the surface induce forces on the probe that bend the cantilever. The deflection is measured using a laser spot reflected from the top surface of the cantilever into an array of photodiodes, it providing a map of the atoms on the surface. A schematic diagram of AFM is shown in Figure 3.10.

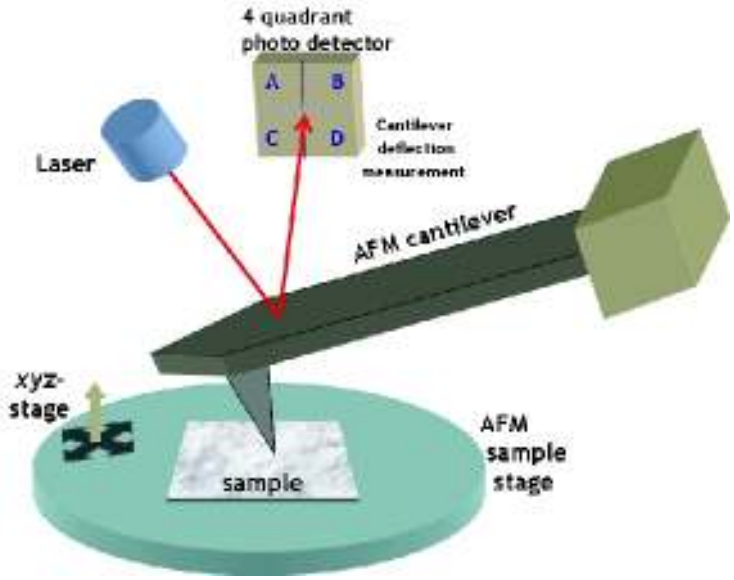

Figure 3.10: Schematic diagram of AFM

If the tip was scanned at a constant height, a risk would exist that the tip collides with the surface, causing damage. Hence, in most cases a feedback mechanism is employed to adjust the tip-to-sample distance to maintain a constant force between the tip and the sample. Traditionally, the sample is mounted on a piezoelectric tube, which can move the sample in the *z* direction for maintaining a constant force, and the *x* and *y* directions for scanning the sample. Alternatively a 'tripod' configuration of three piezo crystals may be employed, with each responsible for scanning in the x, y and z directions. This eliminates some of the distortion effects seen with a tube scanner. In newer designs, the tip is mounted on a vertical piezo scanner while the sample is being scanned in X and Y using another piezo block. The resulting map of the area s = f(x,y) represents the topography of the sample. Atomic force microscopes can achieve magnification of a factor of 5×10^6, with a resolution of 2 angstroms.

In the present study the synthesized thin film samples were used for AFM and 2 dimensional as well as 3 dimensional images were recorded using an NT-MDP (Russian Made), Solver Pro-47 in tapping mode. The size of the particle was directly calculated from the obtained two dimensional images and particle size histogram. In our present study, particle sizes were calculated for pure and 10 mole% doped ZnO (totally 4) nanocrystalline fims.

3.6.4. SEM Measurements

In a scanning electron microscope, the surface of a solid sample is scanned in a raster pattern with a beam of energetic electrons. Several types of signals are produced from a surface in this process. All of these signals have been used for surface studies, but the two most common signals used for surface studies are: (1) backscattered and secondary electrons, which serve as the basis of scanning electron microscopy, and (2) X-ray emission, which is used in electron microprobe analysis.

Figure 3.11 is a schematic of a scanning electron microscope. Scanning with a SEM is accomplished by the two pairs of electromagnetic coils located within the objective lens; one pair deflects the beam in the x-direction across the sample, and the other pair deflects it in the y-direction. Scanning is controlled by applying an electrical signal to one pair of scan coils, such that the electron beam strikes the sample to one side of the center axis of the lens system. By varying the electrical signal to this pair of coils (that is, the x-coils) as a function of time, the electron beam is moved in a straight

line across the sample and then returned to its original position. After completion of the line scan, the other set of coils (y-coils in this case) is used to deflect the beam slightly, and the deflection of the beam using the x-coils is repeated. Thus, by rapidly moving the beam, the entire sample surface can be irradiated with the electron beam. The signals to the scan coils can be either analog or digital. Digital scanning has the advantage that it offers very reproducible movement and location of the electron beam. The signal from the sample can be encoded and stored in digital form along with digital representations of the x and y-positions of the beam.

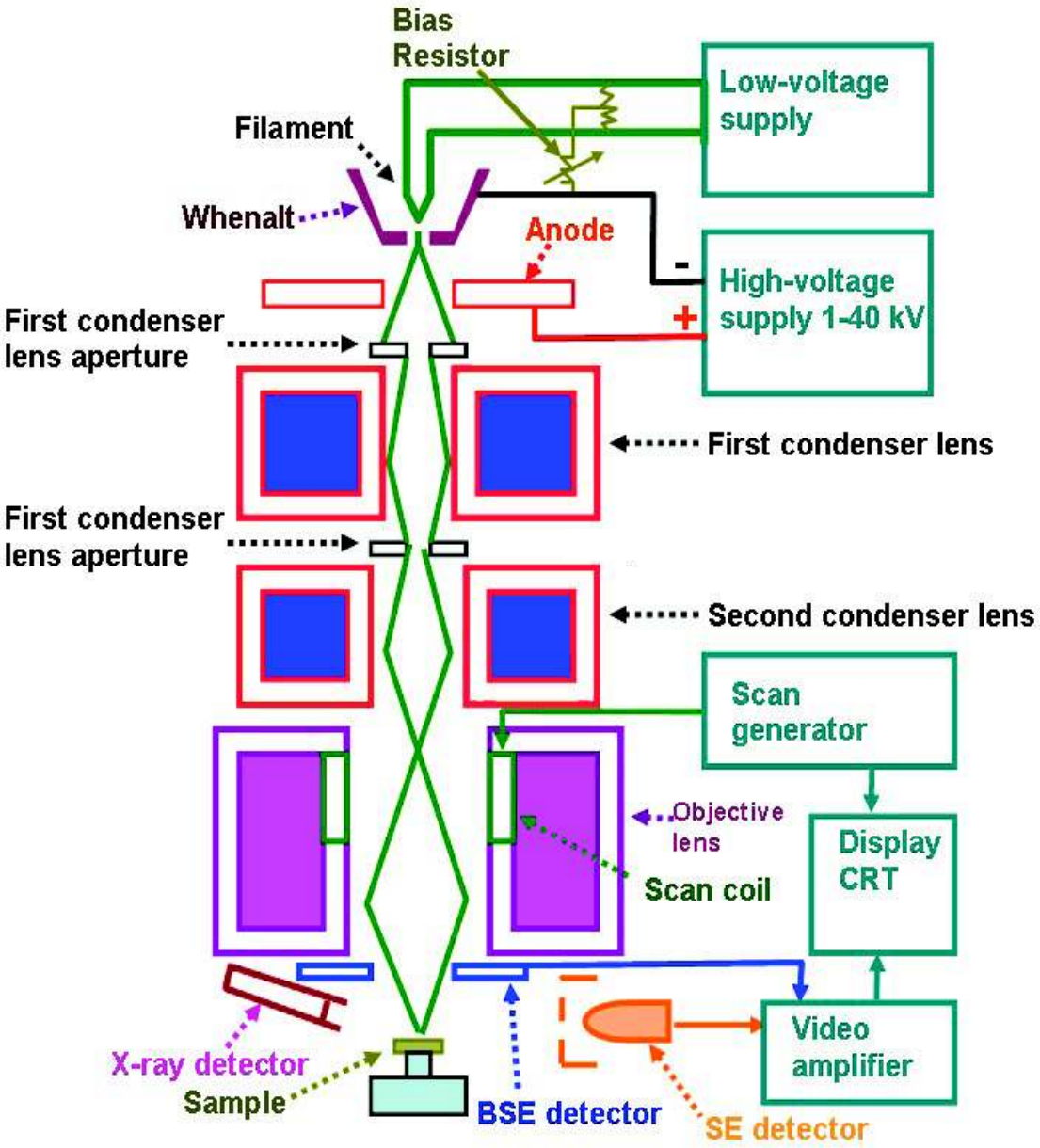

Figure 3.11: Schematic representation of a scanning electron microscope (SEM)

The signals that are used to drive the electron beam in the x and y-directions are also used to drive the horizontal and vertical scans of a cathode-ray tube (CRT). The image of the sample is produced by using the output of a detector to control the intensity of the spot on the CRT. Thus, this method of scanning produces a map of the sample in which there is a one-to-one correlation between the signal produced at a particular location on the sample surface and a corresponding point on the CRT display. The specimen stage is provided with a mechanism whereby the sample can be moved in two mutually perpendicular directions and rotated as well, thus permitting scanning of the surface. The electron microprobe provides a wealth of information about the physical and chemical nature of surfaces. It has important applications to phase studies in metallurgy and ceramics, the investigation of grain boundaries in alloys, the measurement of diffusion rates of impurities in semiconductors, the determination of occluded species in crystals, and the study of the active sites of heterogeneous catalysts. In all of these applications, both qualitative and quantitative information about surfaces is obtained. In our present study, Microstructural analysis has been performed using SEM Zeiss-SUPRA 40 by secondary electron imaging mode.

3.6.5. TEM Measurements

Transmission Electron Microscope (TEM) is an imaging technique whereby a beam of electrons are focused onto a specimen causing an enlarged version to appear on a fluorescent screen or layer of photographic film or can be detected by a camera. The magnification effect would be very clear. TEM is used heavily in both material science/metallurgy and biological sciences. In both the cases the specimens must be very thin and should be able to withstand the high vacuum present inside the instrument. A crystalline material interacts with the electron beam mostly by diffraction rather than absorption. A length calculated bar is provided already inside the TEM picture. Using that scale one can estimate the size of the particle. Sample is dispersed in ethanol (EtOH) and sonicated for 5 minutes. The dispersion is dispersed on a Cu TEM grid and allowed to dry overnight in ambience. This is then analyzed in TEM.

In our present study, TEM measurements were done on the pure ZnO, 10 mole % Mn^{2+} doped ZnO, 10 mole % Cu^{2+} doped ZnO and 10 mole % Pb^{2+} doped ZnO samples using a FEI Tecnai 30 G^2 300 kV, resolution 1.4 Å with 1 million magnification power.

3.7. Optical Measurements

Optical measurements include ultraviolet-visible spectroscopic (UV-Vis) analysis and photoluminescence spectroscopic (PL) analysis. From the UV-Vis analysis we can determine optical bandgap, absorption edge wavelength, band edge sharpness and confirmation of direct/indirect bandgap. Fluorescence emission always gives a broad band. In order to have a sharp and intense band it is customary to use nanosized materials which possess fewer numbers of levels in conduction band. The measurement of fluorescence allows the quantitative determination of traces of many organic and inorganic species.

3.7.1. UV-Vis Spectroscopic Analysis

Ultraviolet-visible spectroscopy or ultraviolet-visible (UV-Vis) involves the spectroscopy of photons in the UV-visible region. This means it uses light in the visible and adjacent (near ultraviolet (UV) and near infrared (NIR)) ranges. The absorption in the visible ranges directly affects the colour of the chemicals involved. In this region of the electromagnetic spectrum, molecules undergo electronic transitions.

The schematic representation of a UV-Vis-NIR spectrophotometer is shown in Figure 3.12. It uses light in the visible and adjacent near ultraviolet (UV) and near infrared (NIR) ranges. In this region of energy, space molecules undergo electronic transitions. The ultraviolet spectrum of a molecule results from transitions between electronic energy levels accompanied by changes both in vibrational and rotational states. The ultraviolet spectrum may be divided into the following regions:

3.7.1a. Far (or Vacuum) Ultraviolet Region

The region from 10-200 nm can be studied in evacuated systems and is termed as “vacuum ultraviolet”. The atmospheric absorptions below 200 nm are a blessing to all, including the spectroscopists, since it prevents the hazardous (high energy) ultraviolet radiation in the sunlight from striking the earth’s surface. In organic molecules, the maximum energy separation occurs when electrons in σ bonds are excited giving rise to absorption in the range 120-200 nm. The range is difficult to measure and is little diagnostic value.

3.7.1b. Near or Quartz Ultraviolet Region

The range from 200-380 nm is the portion of the spectrum normally covered by the term ultraviolet. The atmosphere is transparent in this region and quartz optics may be used to scan from 200-380 nm. The excitation of electrons from p & d orbitals, π-orbitals and particularly π-conjugated systems occurs above 200 nm and gives rise to readily accessible and informative spectra.

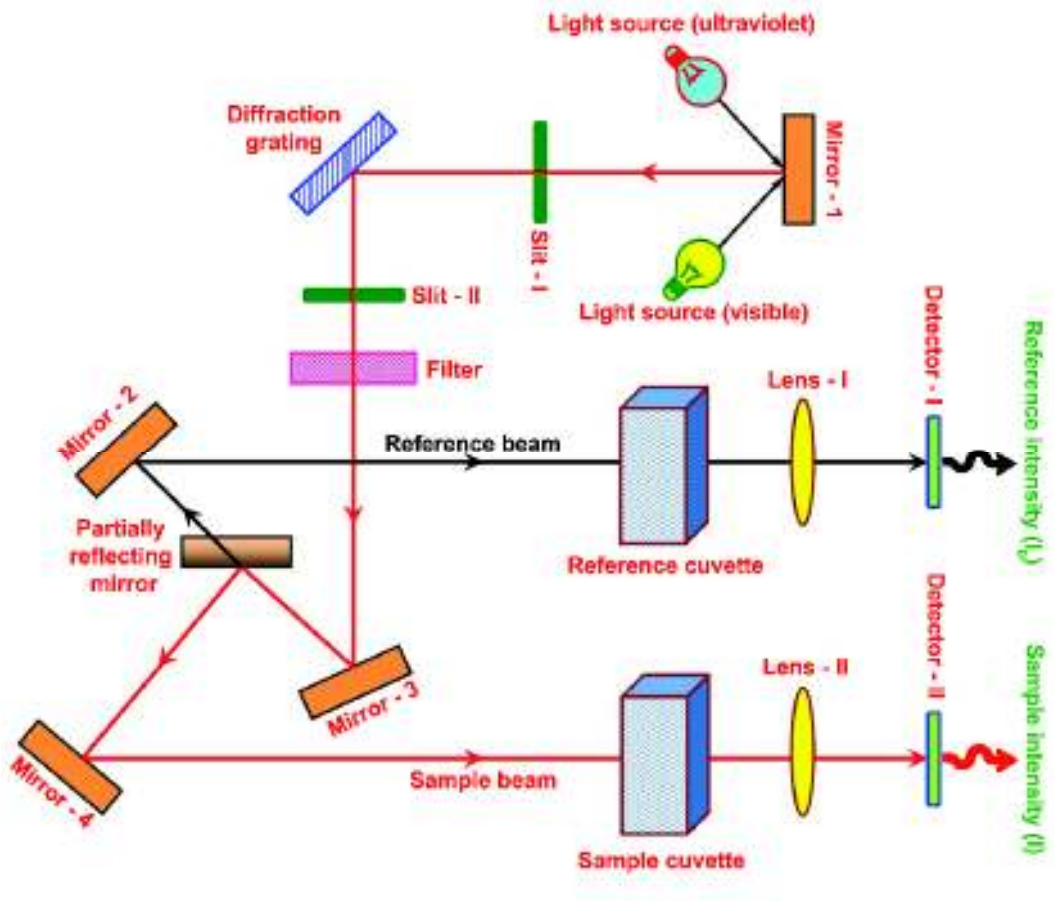

Figure 3.12: Schematic experimental setup for UV-Vis-NIR spectrophotometer

3.7.1c. Visible Region

The spectral range, which is accessible with most instruments, is from 200 nm to 800 nm and this entire region is often referred to as ultraviolet spectrum although it includes the visible region (380 to 780 nm). A tungsten filament lamp is generally used

for the visible region of the spectrum. Conjugation of double bonds lowers the energy required for the transitions and absorption moves to longer wavelength.

In our present study, optical absorption measurements were done at room temperature on the thin film samples using a SHIMADZU UV-2400 PC spectrometer with a medium scan speed sampling interval 0.5 in the wavelength range 200-800 nm.

The fundamental absorption, which corresponds to electron excitation from the valence band to conduction band, can be used to determine the value of the optical bandgap. The absorption coefficient α was determined using the relation,

$$\alpha = \frac{2.303 \log(\text{absorption})}{\text{Thickness of the sample}}.$$

The relation between the absorption coefficient (α) and the incident photon energy (hυ) can be written as (Tauc 1974):

$$(\alpha h\upsilon) = A\left(h\upsilon - E_g\right)^n,$$

where, A is a constant, E_g is the bandgap energy of the material and exponent n depends on the type of transition (Joshi *et al.*, 2003). Here, the transitions are direct so we take n = $^1/_2$. The value of optical bandgap was calculated by extrapolating the straight line portion of $(\alpha h\upsilon)^2$ *vs* hυ graph to hυ axis (Figure 3.13). The band edge sharpness value (B_s) was derived from the slope of the plot of $(\alpha h\upsilon)^2$ *vs* hυ in the range of band-to-band absorption.

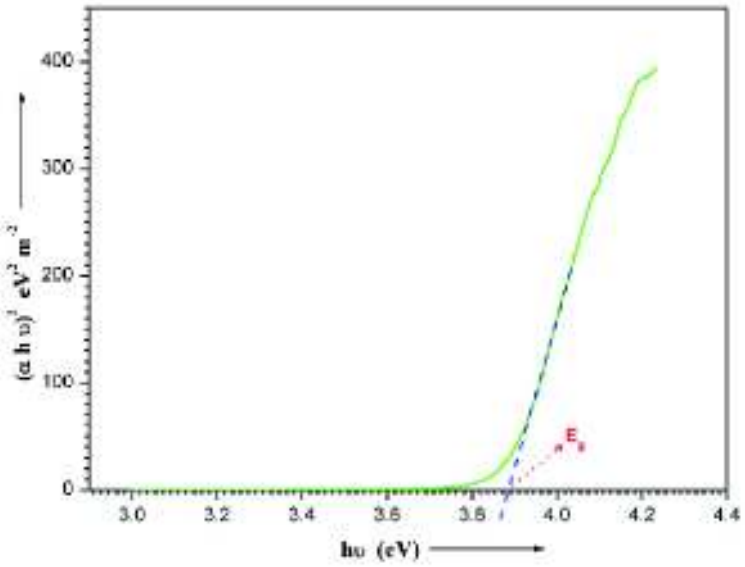

Figure 3.13: Model graph for bandgap energy determination

The following definitions are useful in a discussion of UV-Vis spectroscopy.

* Any group of atoms that absorbs light whether or not a colour is thereby produced is called Chromophore.
* A group which extends the conjugation of a chromophore by sharing of nonbonding electrons is called Auxochrome.
* The shift of absorption to a longer wavelength is called Bathochromic shift.
* The shift of absorption to a shorter wavelength is called Hypsochromic shift.
* An increase in absorption intensity is called Hyperchromic effect.
* A decrease in absorption intensity is called Hypochromic effect.

3.7.2. Photoluminescence Spectroscopic Analysis

This technique is complementary to absorption spectroscopy, in that absorption deals with transitions from the ground state to the excited state, while photoluminescence (fluorescence) measures transitions from the excited state to the ground state.

The two most common manifestations of photoluminescence are: (i) Fluorescence and (ii) Phosphorescence, which are produced by somewhat different mechanisms.

The major difference between fluorescence and phosphorescence process is that in fluorescence the luminescent process stops immediately when the irradiation is stopped but in phosphorescence the process of emission continues for an easily detectable length of time even after the irradiation is discontinued.

The basic elements of a PL spectroscopy set-up consist in an optical source, a spectrophotometer and a detector. A typical PL set-up is shown in Figure 3.14.

Photoluminescence spectroscopy is a contact-less, versatile, non-destructive method of probing the electronic structure of a material. Typically, a laser beam impinges a sample, where it is absorbed. The excess energy brought to the material can be dissipated through the emission of light, or luminescence. As the excitation of the sample is performed by light, this luminescence is called “photoluminescence”. Photoluminescence (PL) is thus the spontaneous emission of light from a material under optical excitation. This light can be collected and analyzed spectrally, spatially

and also temporally. In fact, PL spectroscopy gives information only on the low-lying energy levels of the investigated system. In semiconductor systems, the most common radioactive transition is between states in the conduction and valence bands, with the energy difference being known as the bandgap. During a PL spectroscopy experiment, excitation is provided by laser light with energy much larger than the optical bandgap. The photo-excited carriers consist in electrons and holes, which relax toward their respective band edges and recombine by emitting light at the energy of the bandgap.

The radiative transitions in semiconductors may also involve localized defects or impurity levels. In that case, the analysis of the PL spectrum leads to the identification of specific defects or impurities, and the magnitude of the PL signal allows determining their concentration.

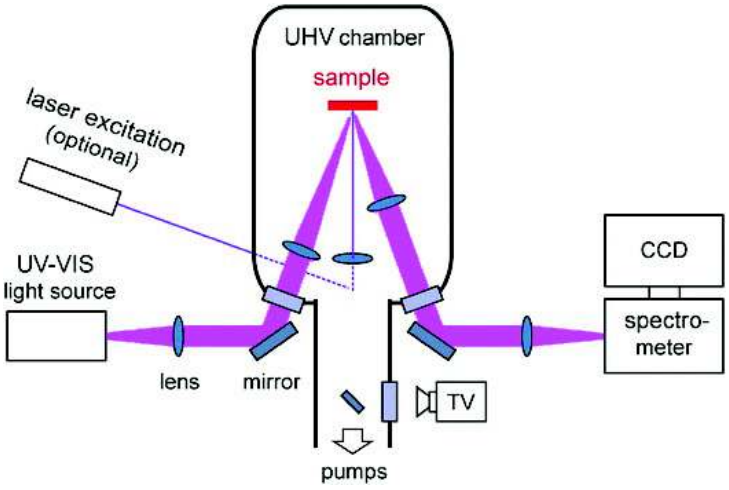

Figure 3.14: Basic scheme of a photoluminescence spectroscopy experimental set up

In all photoluminescence (PL) studies there is a host material which is generally semiconducting. When its bandgap is excited it exhibits fluorescence particularly from the lowest as well as the highest levels of conduction band. As a result the fluorescence emission always gives a broad band. In order to have a sharp and intense band It is customary to use nanosized materials which possess few numbers of levels in conduction band.

The photoluminescence (PL) measurement was carried out for all the 13 thin film samples prepared in the present study by using a FLUOROLOG-FL3-11 Spectroflorometer.

3.8. Photoconductivity Studies

Photoconductivity is an important property of solids by means of which the bulk conductivity of the sample changes due to incident radiation. Photoconductivity is not an elementary process in solids. Photoconduction, as the name suggests, includes the generation and recombination of charge carriers and their transport to the electrodes. Obviously, the thermal and hot carrier relaxation process, charge carrier statistics, effects of electrodes, and several mechanisms of recombination are involved in photoconduction. Above all, every mechanism mentioned is a complicated one, and therefore photoconductivity in general is a very complex process. In spite of the complexity of the photoconductivity process, it provides useful and valuable information about physical properties of materials and offers applications in photo detection and radiation measurements. Historically, Smith and Rose (1955), who observed that the resistivity of selenium was decreased by radiation falling on it, recorded the first photoconductivity effect in 1873. According to the literature, this is the very first experimental detection of photoconductivity (Joshi 1990).

Einstein's explanation of the photoelectric effect opened the way to interpreting the interaction of radiation with matter, particularly optical absorption, photoconductivity, the photovoltaic effect and other related phenomena.

The basic principle involved in photoconductivity is often stated in a very simple way. When photons of energy greater than that of the band gap of the material are incident upon a photoconductive material, electrons and holes are created in the conduction and valence bands, respectively increasing the conductivity of the sample. But this statement is only partially true. In a doped material, for example, the impurity atom absorbs the photon of slightly less energy than that of the band gap and free electron is created in the conduction band (Bube 1960).

Since last decades the photoconductivity properties of inorganic nanoparticles have become subject of intensive study (Bera and Basak 2008; Maurya *et al*., 2011) not only because of fundamental interests in the nature of the electronic excitations but also due to their applications in wide range of optical and electronic devices. In semiconductors, photoconductivity arises due to generation of electron–hole pairs as a result of interaction of photons with bound electrons of lattice atoms. Photoconductivity of material depends upon the carrier density, carrier lifetime and complex processes of

carrier generation, trapping, and recombination. Photoconductivity is also a function of temperature, applied field, intensity of light and energy of radiation (Joshi 1990; Kripal *et al*., 2010).

3.8.1. Photoconduction

In short, photoconductivity is due to the absorption of photons (either by an intrinsic process or by impurities with or without phonons), leading to the creation of free charge particles in the conduction band and/or in the valence band. Photo absorption and hence photoconduction takes place by one of the following mechanisms.

(i) Band-to-band transitions
(ii) Impurity levels to band edge transitions
(iii) Ionization of donors
(iv) Deep level (located in the valence band) to conduction band transitions.

3.8.2. Dark Conduction

Dark current (dark conduction), I_d, is the amount of current that flows through the material or device when no radiation is incident on it. It changes with operating temperature and applied voltage, and therefore these parameters should be always mentioned. Dark current is not a constant background current but also has fluctuations or noise. The average dc value of the current is generally mentioned as dark current.

3.8.3. Negative Photoconductivity

In few cases, it has been observed that when radiation of certain energy is incident on a photoconductor, a decrease in current is observed instead of the expected increase; this phenomenon is called “negative photoconductivity”. The variation in the mobilities of charge carriers is generally very small (here two-dimensional materials excluded) and hence can be ignored. This means that either the number of free charge carriers or their life time is substantially reduced by incident radiation (Joshi 1990).

3.8.4. Positive Photoconductivity

Photoconductive materials usually exhibit an increase in conductivity under illumination which is a direct result of the absorption of photon energy greater than band-gap of material. This phenomenon is known as positive photoconductivity (Bhushan and Sharma 1990; Winiarz *et al*., 1999).

3.8.5. Experimental Setup

The thin film sample is mounted in a specially arranged slide holder. The dark current (I_d) and photocurrent (I_p) was with respect to field voltage. Voltage dependence of dark-current and photocurrent is measured using a digital dc nano-ammeter. The time-resolved rise and decay of photocurrent spectra are recorded using RISH Multi 15S with adapter RISH Multi SI-232. The experimental arrangement is shown in Figure 3.15. In order to obtain the dark current (I_d) and photocurrent (I_p) response of the nanocrystalline film, two metals contacts (copper electrodes) were deposited onto the film using silver paint. Now the metal contact deposited film is pressed with a glass plate for providing illumination area of 0.25 cm^2. The illumination area was properly shielded from all radiation. After shielding the film from all radiation, the film is kept in the dark for several hours. After that a stabilized dc field (5–50 V/cm) is applied across the films through the metal electrodes. The applied voltage was increased from 0 to 50 V insteps of 5 V. Voltage dependence of dark-current (I_d) is measured by using a digital dc nano-ammeter. In order to obtain the photocurrent (I_p) response of the nanocrystalline film, the light illumination (Hg lamp of 300 W is used as photo-excitation source at 580 nm excitation wavelength) is allowed to fall over the film on the illumination area (0.25 cm^2) through a slit. The photocurrent is noted for varying applied fields as before. The photoconductivity measurements was carried out for all the 13 thin film samples prepared in the present study

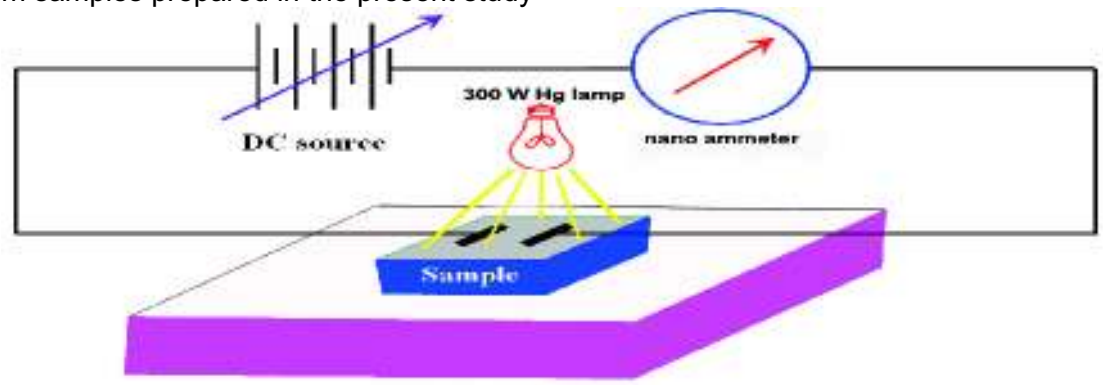

Figure 3.15: Experimental set up for photoconductivity measurements

3.9. Electrical Measurements

One important electrical properties of the solid is its electrical conductivity. The electrical conductivity of a solid is due to the mobility of electrons or ions or imperfections which are charged. In the case of semiconductors, the conductivity is due to the movement of electrons and holes. Electrical measurements include DC electrical, dielectric and AC electrical conductivity measurements. The synthesized thin film samples were directly inserted into the two probe setup.

3.9.1. DC Electrical Measurements

The thin film samples were annealed for two hours at ~60ºC to achieve densification. After the sintering process, the samples were inserted into the four probe arrangement. The DC electrical conductivity measurements were carried out to an accuracy of ± 1% for all the 13 synthesized thin film using the conventional four-probe technique. The measurements were made at various temperatures ranging from 30 - 150ºC

The resistances of the thin film samples were measured using a four probe technique. The samples were again annealed in the holder assembly at ~160ºC before making observations. The observations were made while cooling the sample. Temperature was controlled to an accuracy of ± 0.5ºC. The voltage drops (V) across the samples were measured at constant current (I). The thickness of the thin film samples were measured using a thin film thickness measuring unit model US M probe Vis. spectroscopic reflectometer. The DC conductivity (σ_{dc}) of the crystal was calculated using the relation

$$\sigma_{dc} = \frac{I}{V\, 2\, \pi\, S} \quad \text{mho m}^{-1},$$

where V is the measured voltage drop across the sample, S is the surface area covered by the electrode on the thin film sample

3.9.2. AC Electrical Measurements

In the presence of applied electric field dielectric materials have permanent or induced dipoles. The dielectric constant is one of the basic electrical properties of solids. The capacitance created by the presence of the material is directly related to the dielectric constant (ε_r) of the material. Another important property of a dielectric material is its ability to support an electrostatic field while dissipating minimal energy in the form of heat. When an electric field acts on any matter the later dissipates a certain quantity of electrical energy that transforms into heat energy. This phenomenon is known as loss of power. The amount of power losses in a dielectric under the action of the voltage applied to it is commonly known as dielectric loss ($\tan\delta$).

The measurements of dielectric constant and loss as a function of frequency and temperature are of interest both from theoretical point of view and from the applied physics. Dielectric constant can be measured by determining the change in the capacitance of specially designed condenser when the dielectric is inserted between the plates of that condenser. The dielectric constant determines the share of the electric stress which is absorbed by the material without any dielectric breakdown. Practically the presence of a dielectric between the plates of a condenser enhances the capacitance. This enhancement of capacitance provides the basic experimental method for the measurement of dielectric constant.

Various polarization of dipoles and space charge polarizations can be understood very easily by studying the dielectric properties as a function of frequency and temperature for solids (Wagner *et al*., 1950, Rao *et al*., 1965, Govinda *et al*., 1975). We have several methods available for the measurement of dielectric constant and dielectric loss. Nature of the specimen and the frequency range in which the measurement is desired will determine the method to be adopted (Hill *et al*., 1969). Use of bridges is common in the frequency range of few Hz to 10 MHz.

The capacitance (C) and dielectric loss factor ($\tan\delta$) measurements were carried out to an accuracy of ± 1 % with Agilant 4284A LCR meter in the various temperatures of 30 – 150 ºC and with different frequencies ranges from 100 Hz to 1 MHz by using conventional two-probe technique (Praveen *et al*., 2005; Mahadevan *et al*., 2008; Selvarajan *et al*., 2006; Saravanan *et al*., 2011; Saravanan *et al*., 2012). The experimental setup for electrical analysis is shown in Figure 3.16. The samples were

prepared and annealed in a way similar to that followed for the dc conductivity measurement (see section 3.8.1). The observations were made while cooling the sample. Temperature was controlled to an accuracy of ± 1ºC. Air capacitance (C_{air}) was also measured. The dielectric constant (ε_r) of the crystal was calculated using the relation,

$$\varepsilon_r = \frac{C}{C_{air}}$$

Figure 3.16: Experimental setup for electrical analysis (Agilant 4284A LCR meter)

The AC electrical conductivity (σ_{ac}) was calculated using the relation

$$\sigma_{ac} = \varepsilon_o \varepsilon_r \omega \tan\delta,$$

where ε_o is the permittivity of free space (8.854 x 10^{-12} F/m) and ω is the angular frequency (ω = 2πf; f = 100Hz to 1 MHz in the present study).